

Statistical Channel Model for 60 GHz WLAN Systems in Conference Room Environment

Alexander MALTSEV¹, Roman MASLENNIKOV², Artyom LOMAYEV¹,
Alexey SEVASTYANOV¹, Alexey KHORYAEV¹

¹ Wireless Standards and Technology Group, Intel Corporation, Turgeneva str. 30, 603024, Nizhny Novgorod, Russia

² Wireless Competence Center, Lobachevski State University of Nizhny Novgorod, Gagarina ave. 23, 603950, Nizhny Novgorod, Russia

alexander.maltsev@intel.com, roman.maslennikov@wcc.unn.ru

Abstract. *In this work, a methodology of statistical channel modeling for 60 GHz WLAN systems is proposed and a channel model for the office conference room environment is developed. The proposed methodology takes into account the most important properties of the indoor 60 GHz propagation channel such as large propagation loss and necessity to use steerable directional antennas by the WLAN stations, quasi-optical propagation nature, clustering structure of the channel, and significant impact of the polarization characteristics. A general mathematical structure of the channel model that supports all the described 60 GHz propagation channel properties is suggested. Then the conference room scenario for 60 GHz WLAN systems is introduced. Development of the inter cluster, intra cluster, and polarization impact modeling parameters is considered in details first explaining the used methodology for each channel modeling aspect and then followed by its application to the conference room scenario. The raw data for the channel model development include the experimental results [1], [2] and ray-tracing simulations for the conference room scenario. The proposed channel modeling methodology and the developed conference room channel model were adopted by the IEEE 802.11ad committee for 60 GHz WLAN systems standardization.*

Keywords

Statistical channel model, 60 GHz WLAN, IEEE 802.11ad.

1. Introduction

Reliable channel models for 60 GHz Wireless Local Area Network (WLAN) systems are necessary to support rapid development, standardization, and introduction into the service of the millimeter-wave WLANs.

Generally, development of a channel model relies on experimental investigations of the corresponding propaga-

tion environments with taking into account foreseen properties of the wireless communication system.

The increase of the carrier frequency of 60 GHz WLANs in more than 10 times in comparison with 2.4 GHz and 5 GHz legacy WLAN systems resulted in qualitative changes in the signal propagation properties. Characteristics of the channel have essential implications for 60 GHz WLAN design and experimental investigations of 60 GHz indoor propagation channels [1]-[3] have revealed several such important properties.

First, small wavelength of the 60 GHz band results in significantly larger propagation loss according the Friis transmission equation. As a consequence, high directional transmit and receive antennas have to be used to compensate for the larger propagation loss to sustain operation over typical WLAN distances of up to several tens of meters. Support for mobile and nomadic systems requires the antennas to be electronically steerable. Hence, the channel model should take into account spatial (angular) coordinates of the channel rays at the transmit and receive sides and also support application of any type of the antenna technology (i.e. non-steerable antennas, sector-switching antennas, antenna arrays).

Second, as confirmed by [1], [3], the 60 GHz propagation channel has a quasi-optical nature. The propagation due to diffraction is not significant and not practically viable. Most of the transmission power is propagated between the transmitter and the receiver through the Line-Of-Sight (LOS) and low-order reflected paths. To establish a communication link, the steerable directional antennas have to be pointed along the LOS path (if available) or one of the reflected paths. An additional consequence of the quasi-optical propagation nature is that image based ray-tracing can be an effective means for prediction of spatial and temporal analysis of the channel paths and may be used to assist the channel modeling.

Third, it should be noted that with ideal reflections, each propagation path would include only a single ray. However, as demonstrated by experimental investigations [1], each reflected path actually consists of a number of

rays closely spaced to each other in the time and angular domains due to fine structure of the reflecting surfaces. Hence, the clustering approach [5] is directly applicable to channel models for 60 GHz indoor WLAN systems with each cluster corresponding to the LOS or Non-Line-Of-Sight (NLOS) reflected path.

Fourth, another important aspect of the 60 GHz propagation that should be adequately taken into account in the channel modeling is polarization characteristics. As demonstrated by experimental studies with 60 GHz WLAN prototypes [1], [2], the power degradation due to polarization characteristics mismatch between the antennas and the channel can be as high as 10-20 dB. The physical reason for high polarization impact is that with application of high directional steerable antennas typically only a single LOS or NLOS path will be essentially used for signal transmission and even NLOS signals remain strongly polarized at the receiver.

In this work, a methodology for development of a channel model for 60 GHz WLAN systems that takes into account all the above characteristics of the indoor millimeter-wave channel is proposed and the channel model for the conference room scenario is developed. Section 2 introduces a general mathematical structure of the model suitable for support of all the model properties. The conference room scenario is described in section 3. Section 4 proposes a methodology for modeling inter cluster parameters of the channel and then section 5 derives the inter cluster parameters for the conference room channel model. The polarization impact modeling approach is explained in section 6 and section 7 applies the approach to the polarization effects modeling in the conference room scenario. The intra cluster parameters of the conference room channel model are described in section 8. Section 9 concludes the paper.

2. General Mathematical Structure of Statistical Channel Model

The proposed general mathematical structure of the channel model is given by equation (1). In (1), h is the generated channel impulse response; $t, \varphi_{tx}, \theta_{tx}, \varphi_{rx}, \theta_{rx}$ are the time and azimuth and elevation angles at the transmitter and receiver, respectively. The channel impulse response h is a sum of multiple channel clusters. $\mathbf{H}^{(i)}$ is a 2x2 matrix gain of the i -th cluster describing its polarization characteristics (as explained in section 6) and $C^{(i)}$ is the channel impulse response for the i -th cluster. $\delta(\cdot)$ is the Dirac delta function. $T^{(i)}, \Phi_{tx}^{(i)}, \Theta_{tx}^{(i)}, \varphi_{rx}^{(i)}, \Theta_{rx}^{(i)}$ are the time-angular coordinates of the i -th cluster. $\alpha^{(i,k)}$ is the amplitude of the k -th ray of the i -th cluster $\tau^{(i,k)}, \varphi_{tx}^{(i,k)}, \theta_{tx}^{(i,k)}, \varphi_{rx}^{(i,k)}, \theta_{rx}^{(i,k)}$

are relative time-angular coordinates of the k -th ray of the i -th cluster. Time, angular, and amplitude positions of the clusters are defined in the absolute coordinate systems, associated with the mutual transmitter and receiver location. Positions of individual rays inside the cluster are calculated relative to the coordinates of the cluster.

Based on experimental results and theoretical analysis of the phenomenon, the polarization characteristics of the model were introduced at the cluster level, assuming that all rays comprising one cluster have (approximately) the same polarization characteristics.

It may be seen that the structure of the channel model (1) allows meeting all the requirements discussed in the introduction. The clustering structure of the channel and the polarization characteristics modeling are supported and any kind of the antenna technology (including antennas arrays and sectorized antennas) can be used with the channel model.

3. Conference Room Scenario

Communications in a conference room constitute a typical scenario for 60 GHz WLAN systems deployment in the office environment. This scenario was considered for experimental measurements described in [1], [2], which were performed in the conference room with dimensions 3 m x 4.5 m x 3 m (W x L x H). Those measurements provided the data for the development of the statistical conference room channel model described in this work.

The 3D model of the scenario is shown in Fig. 1. This model corresponds to the experimental setup of [1], [2], and was also used for ray-tracing simulations performed to support the channel model development. The two stations located on the table in the middle of the conference room are communicating to each other using either LOS or first and second reflected propagation paths. The distribution of the stations locations over the table surface is uniform. Averaging over different locations is used to derive a statistical channel model where only the distance between the stations is kept as a model input parameter. The distance is used to define the LOS ray time-of-arrival and attenuation and then also indirectly impacts the characteristics of the NLOS rays that are calculated relative to the LOS ray coordinates. The LOS (with all clusters potentially available) and NLOS (with the LOS ray being blocked) subscenarios are supported by the channel model.

The conference room scenario as described in this section was adopted by the IEEE 802.11ad standardization committee as a mandatory scenario for candidate 60 GHz WLAN systems evaluation [4], [6].

$$\begin{aligned}
 h(t, \varphi_{tx}, \theta_{tx}, \varphi_{rx}, \theta_{rx}) &= \sum_i \mathbf{H}^{(i)} C^{(i)}(t - T^{(i)}, \varphi_{tx} - \Phi_{tx}^{(i)}, \theta_{tx} - \Theta_{tx}^{(i)}, \varphi_{rx} - \Phi_{rx}^{(i)}, \theta_{rx} - \Theta_{rx}^{(i)}) \\
 C^{(i)}(t, \varphi_{tx}, \theta_{tx}, \varphi_{rx}, \theta_{rx}) &= \sum_k \alpha^{(i,k)} \delta(t - \tau^{(i,k)}) \delta(\varphi_{tx} - \varphi_{tx}^{(i,k)}) \delta(\theta_{tx} - \theta_{tx}^{(i,k)}) \delta(\varphi_{rx} - \varphi_{rx}^{(i,k)}) \delta(\theta_{rx} - \theta_{rx}^{(i,k)})
 \end{aligned} \tag{1}$$

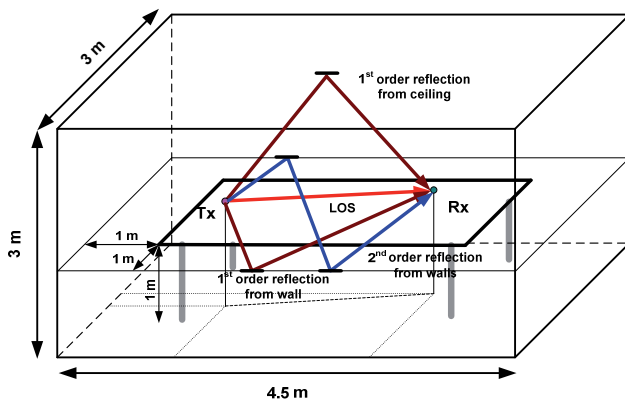


Fig. 1. 3D model of the conference room.

4. Inter Cluster Parameters Modeling Methodology

As explained in the introduction, the clustering approach is naturally applicable to 60 GHz indoor channel modeling and different clusters of the channel correspond to different LOS and low-order reflections propagation paths. In the proposed approach, inter cluster parameters (positions of the clusters in the temporal and spatial domains) are modeled statistically. Statistical models need to be developed for every inter cluster parameter.

Derivation of the statistical models may be based directly on the results of experiments. However, it is proved by experimental measurements [1], [3], that space-time positions of different clusters for the 60 GHz indoor radio channel can be accurately predicted using ray-tracing simulations. (The RMS deviation of the clusters measured and predicted angular coordinates is below 10^0 [1]). Hence, given that the amount of experimental data is usually limited, ray-tracing techniques may be used to generate the inter cluster characteristics (clusters time of arrival, azimuth and elevation angles of arrival and departure) for the channel model. This approach was adopted in the developed methodology. Ray-tracing simulations were performed for the considered environments and then results of the simulations were processed to develop statistical models for different inter cluster parameters. Exploitation of ray-tracing approach allows for significant increase in available channel clusters realizations. For example, in the conference room channel model considered in this paper, the application of ray tracing approach allowed to increase the number of channel realizations from 15 experimental realizations (each requiring exhaustive 4-dimensional scanning with directional antennas in the azimuth and elevation angle planes of the transmitter and receiver [1]) to 100 000 simulated ray-tracing realizations.

Another important property of the inter cluster parameters following from the quasi-optical type of the

propagation is that for a considered environment, a set of the available clusters may usually be divided into several groups with clusters from different groups having essentially different properties. For example, in the considered conference room scenario, there may be five first order reflected clusters for a pair of the transmitter and receiver – four first-order reflections from walls and a single cluster reflected from the ceiling. (The reflection from the floor is blocked by the table). The clusters reflected from walls will have essentially different distributions of inter cluster parameters than the cluster reflected from the ceiling and this has to be taken into account in the channel modeling. It should be noted that parameters of clusters within one group may statistically depend on each other and should be generated jointly. Real environments may have much more complicated structure of the clusters. However, it is still possible to define groups of clusters with essentially different parameters and develop statistical models of the inter cluster parameters separately for each group of clusters. The proposed channel model development methodology uses this approach as illustrated for the conference room channel model below.

Except for the spatial and temporal parameters, statistical models for the gain of the clusters have to be introduced to complete the inter cluster parameters definition. In the proposed channel modeling methodology, the gain of LOS clusters is calculated deterministically by the Friis transmission equation using the separation distance between the transmitter and receiver as a parameter.

For the NLOS clusters, the gain is calculated as the propagation loss along the corresponding NLOS path (the distance of the path may be obtained with the help of ray-tracing) and an additional loss due to reflection. The reflection loss cannot be predicted by the ray-tracing and a statistical model for the reflection loss has to be defined from experimental data.

In addition, the gain of the clusters is impacted by polarization characteristics of the channel and antennas. In this work, the polarization characteristics of the propagation are modeled at the cluster level and may be generally considered as part of the inter cluster parameters. However, the developed methodology for polarization characteristics modeling is treated separately in section 6 of the paper.

Concluding the inter cluster parameters modeling methodology section, it should be noted that not all the clusters present in an empty conference room may be available at each moment, some of the clusters in the scenario may be blocked by moving, standing, and sitting people or some other obstacles. This effect can also be accounted in the channel modeling by introduction of either static (at the duration of a channel drop) or dynamic cluster blockage effects. However, the cluster blockage modeling methodology is a separate problem and is not considered in details in this work. The methodology appropriate to be used with the conference room channel model can be found in [7], [8].

5. Inter Cluster Parameters for Conference Room Channel Model

5.1 Inter Cluster Structure for Conference Room Scenario

A ray tracing model of the conference room was used to generate multiple realizations of the LOS and first and second order reflected clusters to investigate the inter cluster structure for the considered environment. As a result of the inter cluster structure analysis, all the clusters were divided into the five groups (as given by Tab. 1), where clusters in the same group have similar properties.

Type of clusters	Number of clusters
LOS path	1
First order reflections from walls	4
Second order reflections from two walls	8
First order reflection from ceiling	1
Second order reflections from the walls and ceiling	4

Tab. 1. Inter cluster structure of the conference room channel model.

The five groups of clusters defined for the considered scenario include: the LOS ray, first order reflections from walls, first order reflections from ceiling, second order reflections from walls, and second order reflections from walls and ceiling. The reflections from the floor are not taken into account as they are assumed to be blocked by the table. As explained in the methodology description above, different statistical models need to be used for different groups of clusters to enhance the accuracy of the channel model.

5.2 LOS Ray

LOS cluster consists of a single ray with the gain calculated by the Friis transmission equation. The LOS cluster has zero transmit and receive azimuth and elevation angles and also zero Time-Of-Arrival (ToA). Transmit and receive elevation and azimuth angles, as well as ToAs for other clusters, are defined relatively to the LOS path.

5.3 Time of Arrival Distribution for Different NLOS Clusters

Time-Of-Arrival (ToA) of different clusters is calculated relatively to the LOS path ToA. Empirical distributions of the ToA for different cluster groups were calculated with the help of ray-tracing simulations. Then piece-wise linear approximations of the empirical probability density functions (PDFs) were used to develop statistical models for the ToA parameters. The empirical PDF obtained from the ray-tracing simulations and the developed approximations of the ToA distributions are shown for the four groups of the NLOS clusters in Fig. 2.

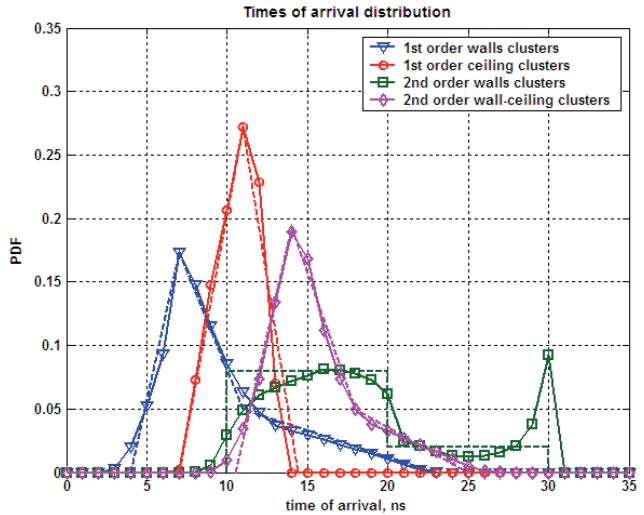


Fig. 2. ToA distributions obtained from the ray-tracing simulations (solid curve) and piece-wise linear approximations used in the conference room channel model (dashed curves).

5.4 Angular Characteristics of First Order Reflections from Walls

Empirical distributions of the angles of departure (AoD) and arrival (AoA) for all cluster groups were generated also with the help of ray-tracing simulations. After that simple linear approximations of the PDFs for the azimuth and elevation angles of departure and arrival were used.

For each channel realization, there are always four clusters corresponding to four first order reflections from the walls (one reflection per wall). An example of four clusters corresponding to the first order reflections from walls is shown in Fig. 3.

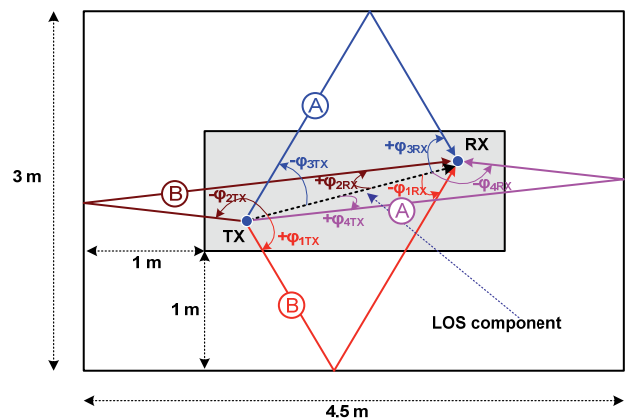


Fig. 3. Example of four clusters corresponding to the first order reflections from walls.

Preliminary analysis revealed that there are a number of properties for this type of clusters following from the geometry that should be taken into account in the channel model. For instance, the elevation angles for all the four

clusters are zero (transmitter and receiver are placed at the same height). Also there is dependence between azimuth angles of the clusters. Two clusters always have positive AoDs and negative AoAs (relatively to the LOS direction) and the other two clusters have negative AoDs and positive AoAs. Moreover, there is dependence between azimuth angles for the two clusters inside each pair (clusters A and B in Fig. 3.). As a result, a procedure for joint generation of the azimuth angles for clusters A and B with the same sign (positive or negative) was developed. The joint 2D distribution of such pairs of angles was calculated with the help of ray-tracing and plotted in Fig. 4.

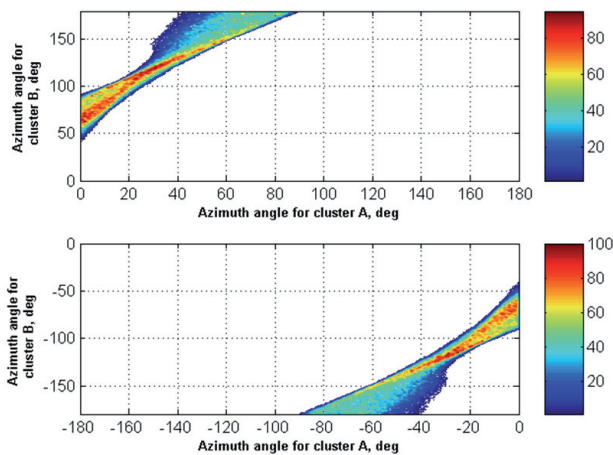


Fig. 4. Joint 2D distribution (histogram) of the azimuth angles with the same sign for two clusters corresponding to the first order reflections from the walls.

As it follows from the histogram in Fig. 4, it is not a uniform distribution and some pairs of angles have greater probability than others. For the sake of simplicity, ray-tracing distributions were approximated in the model by uniformly distributed pairs of angles in trapezoidal areas 1 and 2 as shown in Fig. 5.

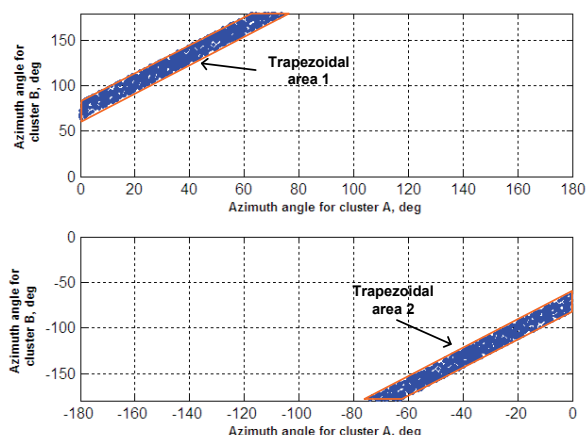


Fig. 5. Approximation of the joint 2D distribution of azimuth angles with the same sign for two clusters corresponding to the first order reflections. The 2D PDFs are uniform in the specified trapezoidal areas.

AoDs and AoAs in each pair of clusters are generated independently only taking into account that the AoD with

smaller absolute value corresponds to the AoA with greater absolute value and the AoD with greater absolute value corresponds to the AoA with smaller absolute value.

The details of the generation procedure for the azimuth angles and rigorous mathematical equations are given in [4].

5.5 Angular Characteristics for First Order Reflections from Ceiling

A single cluster corresponding to the first order reflection from the ceiling takes into account the properties that the azimuth AoD and AoA are equal to zero and that the elevation AoD and AoA are equal to each other. The distribution of the elevation angle obtained with the help of ray-tracing and a linear approximation for the PDF used in the conference room channel model are shown in Fig. 6.

5.6 Angular Characteristics for Second Order Reflections from Walls and Ceiling

Statistical models for inter cluster parameters of the second order reflections from the walls and second order reflections from the walls and ceiling were derived in the same manner with the help of the proposed methodology (see [4] for more details).

As it was verified from ray-tracing simulations second order clusters reflected from walls and ceiling have the following angular properties:

- There are in total four clusters corresponding to the reflections from a wall and then ceiling or from ceiling and then a wall (depends on the relative positions of transmitter and receiver).
- There is exactly one reflection per each wall (either the wall and then ceiling or ceiling and then the wall).
- The azimuth AoD and AoA of these clusters are equal to the azimuth angles generated for the first order reflections from walls described in section 5.4.
- The elevation AoD and AoA are equal to each other as for the first order reflections from the ceiling. The empirical ray-tracing PDFs and channel model approximations are shown in Fig. 6.

5.7 Angular Characteristics for Second Order Reflections from Walls

This group of clusters has the following angular characteristics verified by ray-tracing simulations:

- There are in total eight clusters corresponding to the second order reflections from walls.
- These clusters have zero elevation AoD and AoA (transmitter and receiver are placed at the same height).

- The azimuth AoA for the cluster of this group is either equal to the AoD (for reflection from two parallel walls) or AoD +/- 180° (for reflection from two perpendicular walls).

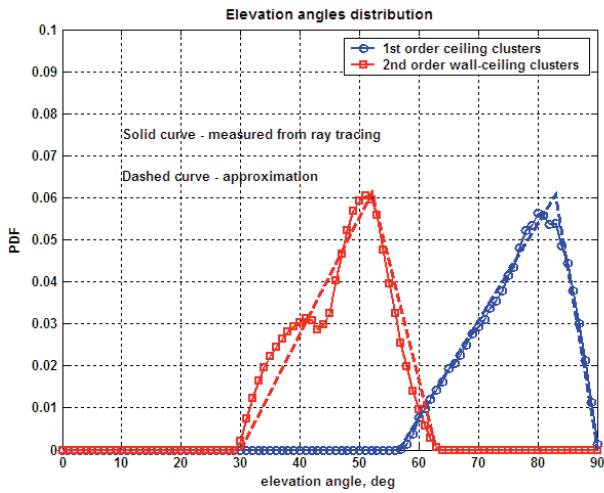


Fig. 6. Empirical ray-tracing PDFs and channel model approximations for elevation angles of first order reflections from ceiling and second order reflections from walls and ceiling.

The joint 2D distribution (histogram) for the azimuth AoD and AoA obtained with the help of ray-tracing simulations is plotted in Fig. 7. At first, this histogram shows that there are in total four different regions in joint distribution of azimuth AoD and AoA angles. It was verified that there are always two clusters pertained to each region. At second, it is not a uniform distribution and some pairs of AoD and AoA angles are more probable than other.

In order to keep the channel model complexity at a reasonable level, the azimuth AoD is generated using uniform distributions in the range of [-180°, 0°] for the regions #1, #2 and [0°, 180°] for the regions #3, #4. The azimuth AoA coincides with AoD for the regions #2 and #3, or equal to AoD + 180° for the region #1 and AoD - 180° for the region #4. The details of the generation procedure for the azimuth angles are provided in [4].

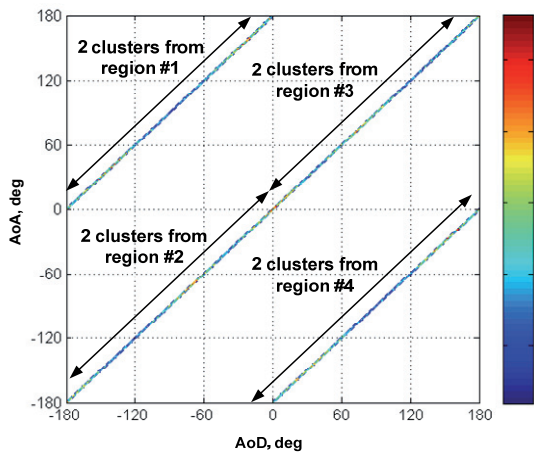


Fig. 7. Joint 2D distribution (histogram) for the azimuth AoD and AoA angles for second order wall reflections.

5.8 Gain of Clusters

Gain of the LOS cluster is calculated as free space attenuation over the corresponding signal propagation path in accordance with Friis transmission equation:

$$G_{LOS} = \lambda / (4\pi d) \tag{2}$$

where λ is a wavelength (5 mm) and d is the distance between transmitter and receiver.

Gain of NLOS clusters takes into account attenuation due to propagation and additional attenuation due to reflection loss:

$$G_{NLOS} = g\lambda / (4\pi(d+R)), R = ct \tag{3}$$

where g is a reflection loss coefficient, R is equal to the product of the NLOS ToA relatively to the LOS ToA obtained from distributions shown in Fig. 2 and the speed of light c .

Statistical models for the reflection loss coefficients for the first and second order reflections are taken as truncated log-normal distributions approximated the experimental distributions measured in [1].

The reflection loss truncated log-normal distribution for the first order reflections has the mean value of -10 dB, the RMS deviation of 4 dB, and the truncation level of -2 dB. Fig. 8 shows a histogram of the measured reflection loss distribution for the first order reflections and the corresponding approximation with the truncated log-normal distribution.

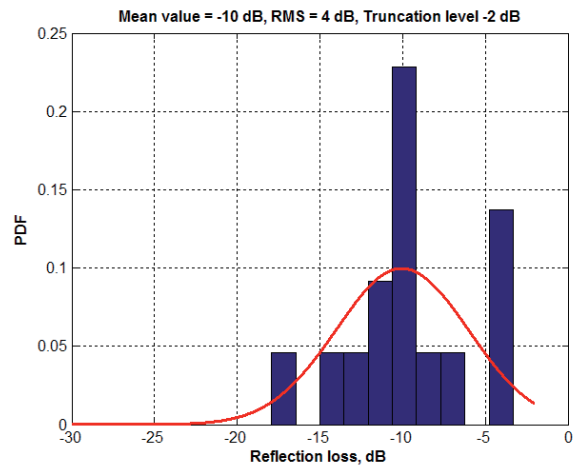


Fig. 8. Histogram of measured reflection loss distribution for the first order reflections and the corresponding approximation with the truncated log-normal distribution used in the channel model.

The reflection loss truncated log-normal distribution for the second order reflections has the mean value of -16 dB, the RMS deviation of 5 dB, and the truncation level of -2 dB. Fig. 9 shows a histogram of the measured reflection loss distribution for the second order reflections and the corresponding approximation with the truncated log-normal distribution.

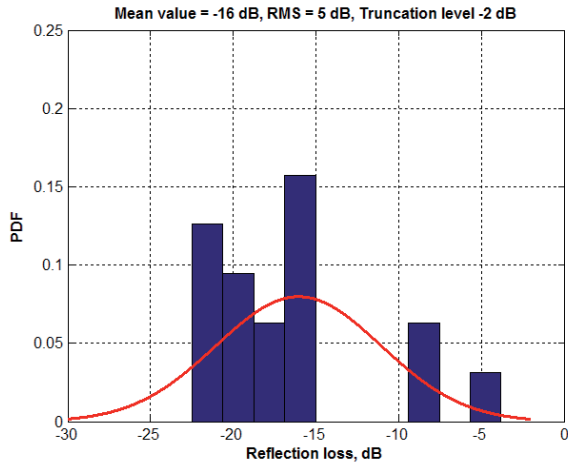


Fig. 9. Histogram of the measured reflection loss distribution for the second order reflections and the corresponding approximation with the truncated log-normal distribution used in the channel model.

6. Polarization Characteristics Modeling Methodology

Unlike the legacy 2.4 GHz and 5 GHz WLAN systems, where polarization characteristics are sometimes omitted in the channel modeling with the assumption of some moderate degradation due to polarization mismatch, 60 GHz WLAN channel models require a detailed support of polarization characteristics of the antennas and the channel since the degradation due to polarization characteristics mismatch can be as large as 10-20 dB [2].

To develop the polarization impact modeling methodology, first, the description of the antenna polarization properties should be introduced. In the far field zone of the EM field radiated by the antenna, the electric vector \mathbf{E} is a function of the radiation direction (defined by the azimuth angle φ and elevation angle θ in the reference coordinate system) and decreases as r^{-1} with increase of the distance r . An illustration of the transmitted \mathbf{E} vector in the far field zone is shown in Fig. 10.

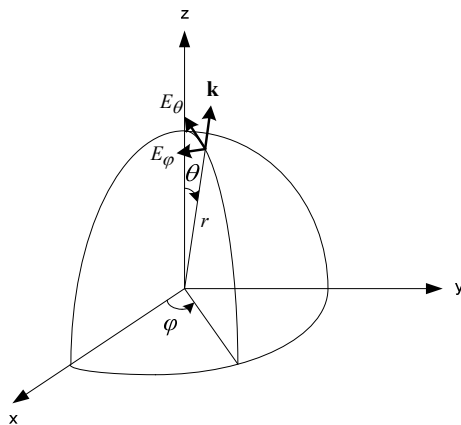


Fig. 10. Transmitted \mathbf{E} vector in the far field zone.

Vector \mathbf{E} is perpendicular to the propagation direction \mathbf{k} and can be decomposed into two orthogonal components: E_θ and E_φ that belong to the planes of constant φ and constant θ angles respectively. Knowledge of E_θ and E_φ of the radiated signal (which may be functions of φ and θ) fully describes polarization characteristics of the antenna in the far field zone.

With the selected \mathbf{E} field bases (E_θ and E_φ components) for the TX and RX antennas, the polarization characteristics of each ray of the propagation channel may be described by a channel polarization matrix \mathbf{H} . In this case, the transmission equation for a single ray channel may be written as:

$$y = \mathbf{e}_{RX}^H \mathbf{H} \mathbf{e}_{TX} x \tag{4}$$

where x and y are the transmitted and received signals, \mathbf{e}_{TX} and \mathbf{e}_{RX} are the polarization vectors (composed of the normalized E_θ and E_φ components) for the TX and RX antennas respectively. Components of polarization matrix \mathbf{H} define gain coefficients between the E_θ and E_φ components at the TX and RX antennas.

For the LOS signal path, matrix \mathbf{H}_{LOS} is close to the identity matrix (non-diagonal components may be non-zero but significantly smaller than diagonal elements) multiplied by the corresponding gain coefficient due to path loss. The LOS propagation does not change polarization characteristics of the signals. However, polarization changes upon the reflection as predicted by the Fresnel laws [9]. Since different clusters of the channel model correspond to different LOS or NLOS reflected paths and the polarization changes only at the reflections, the rays within one cluster are expected to have similar polarization characteristics. For this reason, the polarization impact was modeled at the cluster level with all rays inside one cluster having the same polarization properties.

It is known that reflection coefficients are different for the \mathbf{E} field components parallel and perpendicular to the plane of incidence and depend on the incident angle. Theoretical coupling between parallel and perpendicular components of the reflected signal is zero for plane media interfaces (boundaries). But due to non-idealities (roughness) of the surfaces some coupling always exists in real channels.

An example of a first order reflected signal path is shown in Fig. 11.

The polarization matrix for the first order reflected signal path may be found as a product of the matrix that rotates \mathbf{E} vector components from the coordinate system associated with the TX antenna to the coordinate system associated with the incident plane. Next, reflection matrix \mathbf{R} with reflection coefficients and cross-polarization coupling coefficients is applied, followed by a rotation to the coordinate system associated with the RX antenna. Thus, the channel propagation matrix for the case of the first order reflected signals may be defined as given by (5).

$$\mathbf{H}_{ref1} = \underbrace{\begin{bmatrix} \cos(\psi_{rx}) & \sin(\psi_{rx}) \\ -\sin(\psi_{rx}) & \cos(\psi_{rx}) \end{bmatrix}}_{\substack{\text{recalculation} \\ \text{of polarization} \\ \text{vector from the} \\ \text{plane of incidence basis} \\ \text{to RX coordinates}}} \times \underbrace{\begin{bmatrix} R_{\perp}(\alpha_{inc}) & \xi_1 \\ \xi_2 & R_{\parallel}(\alpha_{inc}) \end{bmatrix}}_{\substack{\text{reflection} \\ \text{matrix} \\ \mathbf{R}}} \times \underbrace{\begin{bmatrix} \cos(\psi_{tx}) & \sin(\psi_{tx}) \\ -\sin(\psi_{tx}) & \cos(\psi_{tx}) \end{bmatrix}}_{\substack{\text{recalculation} \\ \text{of TX polarization} \\ \text{vector to the plane} \\ \text{of incidence basis}}} \quad (5)$$

Incident angle α_{inc} and rotation angle ψ_{tx} are introduced in (5) as shown in Fig. 11. Rotation angle ψ_{rx} is introduced at the receiver in a similar way as ψ_{tx} , at the transmitter. The reflection matrix \mathbf{R} includes the reflection coefficients R_{\perp} and R_{\parallel} for the perpendicular and parallel components of the electric field E_{\perp} and E_{\parallel} respectively. Elements ξ_1 and ξ_2 in the matrix \mathbf{R} are cross-polarization coupling coefficients. Equation (5) demonstrates that there are generally two mechanisms for depolarization (coupling between orthogonal components of the \mathbf{E} vector at the TX and RX sides). These are reflection coupling (coupling between parallel and perpendicular \mathbf{E} vector components at the reflection) and geometrical coupling (coupling because of the different relative orientations of the TX and RX antennas). It may be seen that the proposed approach allows accounting for both mechanisms to create an accurate polarization impact model.

Equation (5) can be generalized for the case of the second order reflections (see [4], [10] for details).

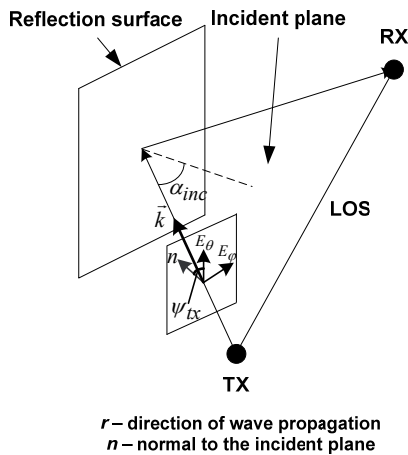


Fig. 11. First order reflected signal path.

To develop statistical models for \mathbf{H} , ray-tracing simulations with support of polarization characteristics are used. Ray-tracing simulations directly account for geometrical depolarization effects associated with different orientations of the transmitter and the receiver polarization bases relative to each other and to the reflecting surfaces. Ray-tracing simulations predict incident angle α_{inc} , rotation angle ψ_{tx} , and rotation angle ψ_{rx} and may capture statistics for the mentioned angles over different relative transmitter and receiver positions. Ray-tracing simulations may also account for cross polarization coupling at the reflection but an adequate experimental based or theoretical model of the reflection matrix \mathbf{R} should be provided.

A detailed description of the proposed polarization modeling methodology is given in [4] and [10]. The work [11] provides results of verification of the model versus experimental data.

7. Support of Polarization Characteristics in Conference Room Channel Model

7.1 Statistical Model for Reflection Matrix

The previous section describes the approach that is proposed for developing polarization impact model. In this approach, the ray-tracing simulations accounting for polarization impact are used to generate empirical distributions of cluster polarization matrices and these distributions are then approximated to create statistical models. However, an unsolved problem from the previous section is how to define coefficients of the reflection matrix \mathbf{R} (needed to simulate reflections in ray-tracing):

$$\mathbf{R} = \begin{bmatrix} R_{\perp} & \xi_1 \\ \xi_2 & R_{\parallel} \end{bmatrix}. \quad (6)$$

One approach is to use dependences for R_{\perp} and R_{\parallel} reflection coefficients on the incident angle predicted by the Fresnel theoretical laws for the flat interface between the regions with refraction indexes n_1 and n_2 . Equations for the perpendicular and parallel coefficients are given by:

$$R_{\perp} = \frac{\sin(\alpha_0 - \alpha_{inc})}{\sin(\alpha_0 + \alpha_{inc})}, \quad R_{\parallel} = \frac{\text{tg}(\alpha_{inc} - \alpha_0)}{\text{tg}(\alpha_{inc} + \alpha_0)} \quad (7)$$

where α_{inc} is an incident angle and α_0 is a function of α_{inc} , n_1 , and n_2 :

$$\alpha_0 = \arcsin\left(\frac{n_1}{n_2} \cdot \sin(\alpha_{inc})\right). \quad (8)$$

Fig. 12 shows the reflection coefficients dependence on the incident angle calculated with the Fresnel formulas for $n_1 = 1$ and $n_2 = 1.8$. The value of the refraction index $n_2 = 1.8$ corresponds to the plasterboard, which is one of the most widely used office materials.

The absolute value of the R_{\perp} constantly grows with the increase of the incident angle and is equal to the unity at the grazing incidence. However, the absolute value of

the R_{\parallel} first decreases with the increase of the incident angle and after achieving the incident angle α_0 (for the given case $\alpha_0 = 61^\circ$) the absolute value of the reflection coefficient starts growing and is equal to the unity at the grazing incidence.

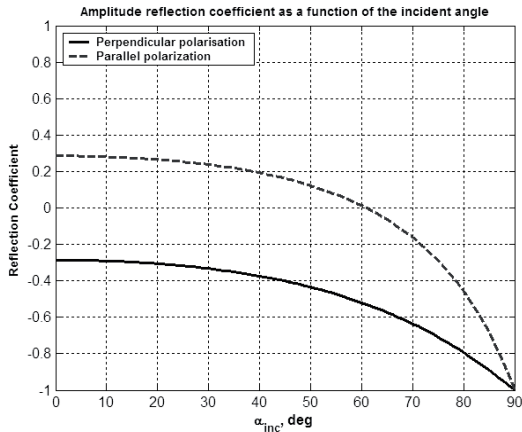


Fig. 12. Reflection coefficients dependence on the incident angle calculated with the Fresnel formulas for $n_1 = 1$ and $n_2 = 1.8$.

But, as it was shown from real experimental measurements, dependences predicted by the Fresnel theoretical laws do not agree well with the measurements results. Experimental investigations of the reflection coefficients versus the incident angle may be found, for example, in [12], where measurements results for typical office surfaces (walls and ceiling) are presented. Since most of the office structures are not uniform (but composed of multiple material layers with different refractive indices), the experimental reflection coefficients have more complex dependence of the absolute value versus the incident angle than it is predicted by the Fresnel laws for a flat boundary of uniform media.

Taking the considerations above into account, the statistical models for the absolute values of the R_{\perp} and R_{\parallel} coefficients were proposed to be independent of the incident angle. The R_{\perp} and R_{\parallel} coefficients were generated using truncated log-normal distribution with the mean equal to -10 dB, the RMS deviation equal to 4 dB, and the truncation level of -2 dB (the same distribution is used for clusters gain modeling in section 5.8). The motivation for using the same statistical law is that the distribution for the clusters gain is based on empirical data of cluster gains averaged over the first order reflections from the walls and ceiling in the conference room [1]. The measurements were done using antennas with linear horizontal polarizations. The geometry of the transmitter and receiver placement in the measurement setup for the considered conference room scenario is such that for the first order reflections from walls, elevation angles of departure and arrival are equal to zero, and for the first order reflections from ceiling the azimuth angles of departure and arrival are equal to zero. As a result, the measured cluster gain values for these cases are directly realizations of the R_{\perp} and R_{\parallel} coefficients (the

rotation matrices of (5) are the identity matrices for these cases). Therefore, the model used to describe the cluster gain values can be used to generate realizations of the absolute values of the reflection coefficients R_{\perp} and R_{\parallel} .

As it follows from the considerations above, the absolute values R_{\perp} and R_{\parallel} are generated as independent statistical variables. This assumption is not quite correct for Fresnel laws but is reasonable when considering experimental dependencies for real surfaces (e.g., [12]). However, both the Fresnel laws and the experimental data demonstrate that handedness of a circularly polarized reflected signal is changed for the incident angles below the α_0 angle and does not change for the incident angles above the α_0 angle. This happens because for the incidence angles below α_0 , the phase of the parallel \mathbf{E} field component is changed by π . This phase shift is responsible for the change of the circular polarization handedness upon reflection at the incident angles below α_0 . This dependence has to be addressed in the channel modeling methodology to be able predict valid polarization impact results. In order to take this effect into account, the signs of the reflection coefficients R_{\perp} and R_{\parallel} were generated in the ray-tracing model as the signs of the reflection coefficient provided by the Fresnel laws for the given incident angle α_{inc} and $n_1 = 1$ and $n_2 = 1.8$ (plasterboard). After performing multiple ray-tracing experiments, the probabilities for the coefficients R_{\perp} and R_{\parallel} to have different combinations of the arithmetic signs were calculated and further used in the development of the statistical models for the polarization matrix \mathbf{H} .

Cross-coupling coefficients ξ_1 and ξ_2 for the matrix \mathbf{R} were modeled as random variables with a fixed absolute value of -20 dB and a random arithmetic sign. The absolute value of -20 dB was estimated from the experimental results presented in [2].

All elements of the matrix \mathbf{H} were generated independently. No statistical dependencies between reflection coefficients R_{\perp} and R_{\parallel} , cross-polarization coupling coefficients ξ_1 and ξ_2 , or between ξ and R were considered because of the relatively small impact provided by the cross-coupling coefficients.

Statistical models for 2x2 polarization matrices \mathbf{H} (from equation (1)) are developed in accordance with the proposed methodology for different types of clusters separately.

7.2 Polarization Characteristics of LOS Ray

Polarization characteristics of the LOS ray are modeled by the polarization matrix \mathbf{H}_{LOS} :

$$\mathbf{H}_{LOS} = \begin{bmatrix} 1 & \xi_1 \\ \xi_2 & 1 \end{bmatrix}. \quad (9)$$

The polarization characteristics of the signal are not altered by the free space propagation. However, in the

general case, the polarization matrix \mathbf{H}_{LOS} will be a rotation matrix of the transformation between the polarizations bases of the TX and RX antennas. In the conference room channel model, the polarization bases of the TX and RX antennas are the same and the rotation matrix is reduced to the identity matrix. Cross-coupling coefficients ξ_1 and ξ_2 are taken with -20 dB absolute value and an equally probable arithmetic sign.

7.3 Polarization Characteristics for First Order Reflected Clusters

Distributions of the polarization matrix \mathbf{H} components for the first order reflections from walls and ceiling obtained with the help of ray-tracing simulations are shown in Fig. 13 and Fig. 14 accordingly.

As it follows from the distributions plotted in Fig. 13 and Fig. 14, H_{11} and H_{22} matrix elements corresponding to reflection coefficients for the E_θ and E_ϕ field components do not change the arithmetic sign. It means that for the considered conference room geometry and chosen area of possible transmitter and receiver positions there are no incident angles for the first order reflections exceeding the angle α_0 .

H_{11} and H_{22} matrix components always have different signs. Physically it means that a circularly polarized signal always changes its handedness after reflection. For example, the left hand circular polarization becomes the right hand circular polarization and vice versa.

It is important to note that the diagonal elements H_{11} and H_{22} of polarization matrix for the first order reflections from walls (see Fig. 13) interchange their places when compared with the same diagonal elements of the polarization matrix for the reflections from ceiling (Fig. 14). It is a consequence of the fact that incident plane is not the same in both cases. In the case of the reflections from walls, the incident plane is the horizontal plane. The electric field component E_θ is perpendicular to the plane of incidence and the component E_ϕ is parallel (pertain to the incident plane). In the case of reflection from ceiling, the incident plane is the vertical one. In that case, the electric field component E_θ becomes parallel (i.e. pertain to the incident plane) and the component E_ϕ becomes perpendicular to the incidence plane.

Due to geometrical properties of the first order reflections from walls (zero elevation angles of departure and arrival), rotation matrices in (5) reduce to the identity matrices and the polarization matrix \mathbf{H} coincides with the reflection matrix \mathbf{R} . There is no geometrical depolarization in this case. As a consequence, the models used to approximate the elements of \mathbf{H} are the same as the models used to generate \mathbf{R} .

The distributions for $|H_{11}|$ and $|H_{22}|$ are truncated log-normal distributions with the mean value of -10 dB, the RMS deviation of 4 dB, and the truncation level of -2 dB. H_{11} always has a negative sign and H_{22} always has a posi-

tive sign. Non-diagonal cross-coupling elements are two equally probable values ± 0.1 in linear scale (-20 dB in log scale).

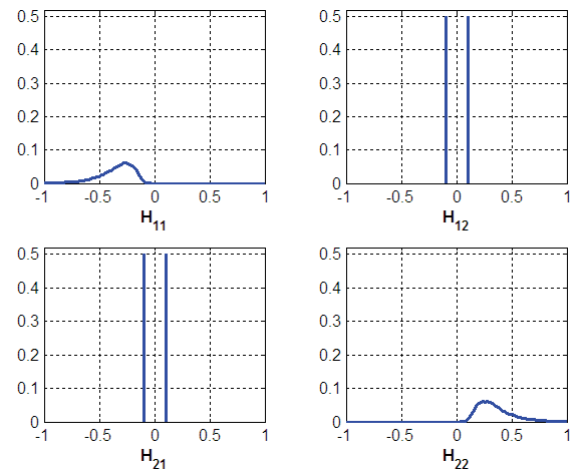


Fig. 13. Distributions of the polarization matrix \mathbf{H} components for the first order reflections from walls.

In the case of the reflection from the ceiling, H_{11} always has a positive sign and H_{22} always has a negative sign.

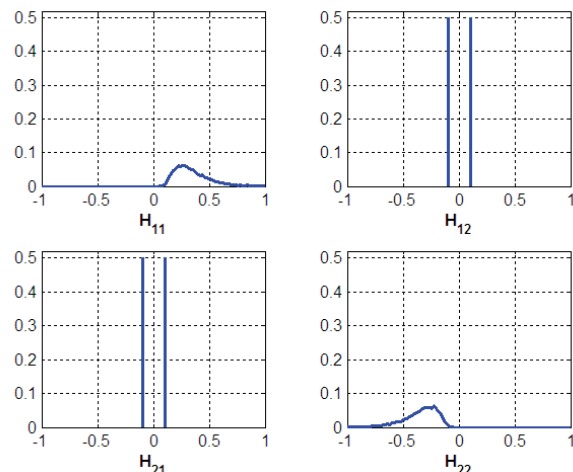


Fig. 14. Distributions of the polarization matrix \mathbf{H} components for the first order reflection from ceiling.

7.4 Polarization Characteristics for Second Order Reflected Clusters

Distributions of the polarization matrix \mathbf{H} components for the second order reflections from walls and ceiling and second order reflections from walls obtained with help of ray-tracing simulations are shown in Fig. 15 and Fig. 16 accordingly.

As it follows from the distributions shown in Fig. 15, H_{11} and H_{22} matrix components for the second order reflections from walls and ceiling do not change the arithmetic sign. It means that, as for the first order reflections, there are no incident angles exceeding the angle α_0 . How-

ever, unlike the first order reflections, H_{11} and H_{22} have the same arithmetic sign. Therefore for this type of clusters circularly polarized signal does not change its handedness after reflection (or actually changes it twice at each of the two reflections).

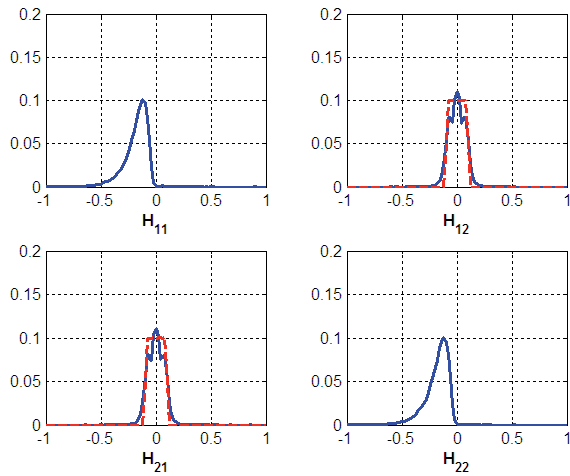


Fig 15. Distributions of the polarization matrix \mathbf{H} components for the second order reflections from walls and ceiling. Solid curves show distributions obtained by ray-tracing, dashed curves show proposed approximations. For the components H_{11} , H_{22} , the proposed approximations provide very close matching to the simulated distributions and the dashed curves are not plotted.

Distributions for the H_{11} and H_{22} matrix components for the second order reflections from walls are plotted in Fig. 16. As it follows from the Fig. 16, H_{22} may be positive or negative with some non-zero probabilities. It means that for this type of clusters incident angle exceeds angle α_0 with some probability and a circularly polarized signal can change its handedness.

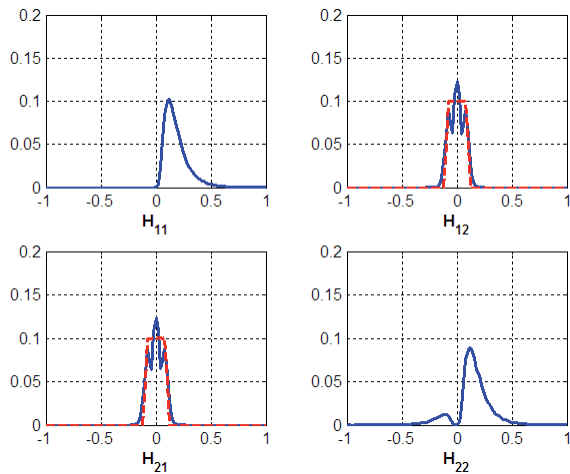


Fig. 16. Distributions of the polarization matrix \mathbf{H} components for the second order reflections from walls. Solid curves show distributions obtained by ray-tracing, dashed curves show proposed approximations. For the components H_{11} , H_{22} , the proposed approximations provide very close matching to the simulated distributions and dashed curves are not plotted.

Distributions for the cross-polarization components H_{12} and H_{21} for the second order reflections obtained from

ray-tracing simulations are not equally probable values ± 0.1 and have distributions shown in Fig. 15 and Fig. 16. For example, for the second order reflections from wall and then ceiling (or from ceiling and then wall) both geometrical depolarization and depolarization at the reflection are present. As a result, it may be seen that channel coefficients between the cross-polarized \mathbf{E} field vector components at the transmitter and receiver are quite significant though essentially below the unity which corresponds to the maximum gain for the co-polarized components of the \mathbf{E} vector.

Statistical distributions of the absolute values of diagonal components for the second order reflections from walls and ceiling $|H_{11}|$ and $|H_{22}|$ are approximated by the truncated log-normal distributions with the mean value equal to -16 dB, the RMS deviation equal to 5 dB, and the truncation level of -2 dB. H_{11} and H_{22} have the same sign and are both negative.

Statistical distributions of the cross-coupling components H_{12} and H_{21} obtained from ray-tracing simulations are approximated by random variables, uniformly distributed in the $[-0.1, 0.1]$ interval.

Statistical distributions of the diagonal components for the second order reflections from walls are approximated as follows. The distribution for $|H_{11}|$ is a truncated log-normal distribution with the mean value equal to -16 dB, the RMS deviation equal to 5 dB, and the truncation level of -2 dB. H_{11} is always positive. The random variable H_{22} is given by:

$$H_{22} = p \cdot X_1 - (1 - p) \cdot X_2 \quad (10)$$

where X_1 and X_2 have the same truncated log-normal distributions as for H_{11} . p is a random variable taking value 1 with probability 0.87 or 0 with the probability 0.13.

Statistical distributions of the cross-coupling components are the same as for the reflections from walls and ceiling.

Distributions of the reflection coefficients for different combinations of the transmitter and receiver polarizations may be found in [4].

8. Intra Cluster Parameters for Conference Room Channel Model

With perfect mirror reflections each cluster will consist of exactly one ray. But taking into account the roughness and heterogeneity of the surfaces as well as the presence of additional small different reflectors each cluster may include several rays closely spaced with each other in time and angular domains.

60 GHz WLAN systems make use of highly directional antennas with narrow beamwidths ($\sim 20^\circ$ - 30°) at both the transmitter and the receiver to overcome the large propagation loss in this band. When the LOS path is pre-

sent, the antennas should be steered along the LOS path for the maximum received signal power. For a NLOS environment, transmitter and receiver apply a beamforming algorithm and steer their antennas toward the best reflected path (cluster) to establish the communication link. In such approach, the transmitter and receiver antennas filter out only one spatial cluster. Hence, the characteristics of the beamformed channel directly depend on the intra cluster parameters. Therefore, accurate modeling of the intra cluster distributions is very important for 60 GHz WLAN systems performance evaluation.

Intra cluster parameters cannot be predicted using ray-tracing and the intra cluster structure should be derived from the measurement data. In the experimental measurements, the identification of the individual rays composing the cluster should be done in both spatial (angular) and temporal domains. From the experimental measurements, it was estimated that the cluster angle dimension is equal to $\sim 5^\circ - 10^\circ$ [13]. Hence, identification of the rays inside of the cluster in the angular domain requires high angular resolution that may be achieved by using directional antennas with very high gain or application of the “virtual antenna array” technique.

For the conference room channel model, a simple model is used to describe the intra cluster angular parameters. Intra cluster azimuth and elevation angles for both transmitter and receiver are modeled as independent normally distributed random variables with zero mean and RMS equal to 5° .

The results of experimental measurements presented in [1], [14] were used to develop the statistical model for the intra cluster time domain distribution. The structure of the intra cluster time domain profile model is schematically shown in Fig. 17. As it follows from this figure, a cluster consists of the central ray $\alpha^{(i,0)}$ with fixed amplitude and pre-cursor $\alpha^{(i,-N_f)}, \dots, \alpha^{(i,-1)}$ and post-cursor rays $\alpha^{(i,1)}, \dots, \alpha^{(i,N_b)}$. For the sake of simulation simplicity, the number of pre-cursor rays N_f and post-cursor rays N_b was derived from measurements and is fixed in the model as $N_f = 6$ and $N_b = 8$.

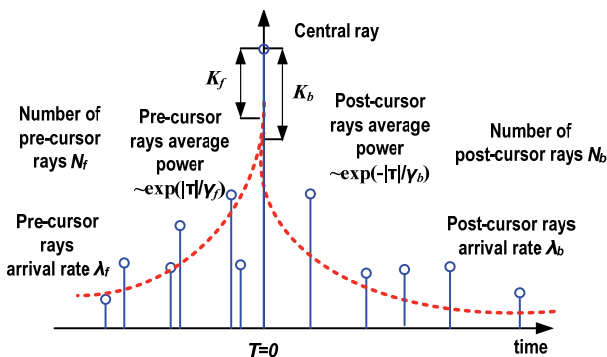


Fig. 17. Structure of the intra cluster time domain profile.

ToAs for the pre- and post-cursor rays are modeled as two independent Poisson processes with the arrival rates $\lambda_f = 0.37 \text{ ns}^{-1}$ and $\lambda_b = 0.31 \text{ ns}^{-1}$, respectively.

The average amplitudes A_f and A_b of the pre-cursor and post-cursor rays decay exponentially with power decay times $\gamma_f = 3.7 \text{ ns}$ and $\gamma_b = 4.5 \text{ ns}$ respectively:

$$A_f(\tau) = A_f(0)e^{-|\tau|/\gamma_f}$$

$$A_b(\tau) = A_b(0)e^{-|\tau|/\gamma_b}$$
(11)

The individual pre-cursor and post-cursor rays $\alpha^{(i,k)}$ have random uniformly distributed phases and Rayleigh distributed amplitudes with the average values A_f and A_b .

The amplitudes of the pre-cursor and post-cursor rays are related to the amplitude of the central ray of the cluster $\alpha^{(i,0)}$ by K -factors that are defined as:

$$K_f = 20 \log_{10} \left| \frac{\alpha^{(i,0)}}{A_f(0)} \right|$$

$$K_b = 20 \log_{10} \left| \frac{\alpha^{(i,0)}}{A_b(0)} \right|$$
(12)

The K -factors are fixed in the model as $K_f = 10 \text{ dB}$ and $K_b = 14.2 \text{ dB}$.

The summary of the used intra cluster time domain parameters for the conference room channel model is given in Tab. 2.

Parameter	Notation	Value
Pre-cursor rays K -factor	K_f	10 dB
Pre-cursor rays power decay time	γ_f	3.7 ns
Pre-cursor arrival rate	λ_f	0.37 ns^{-1}
Pre-cursor rays amplitude distribution		Rayleigh
Number of pre-cursor rays	N_f	6
Post-cursor rays K -factor	K_b	14.2 dB
Post-cursor rays power decay time	γ_b	4.5 ns
Post-cursor arrival rate	λ_b	0.31 ns^{-1}
Post-cursor rays amplitude distribution		Rayleigh
Number of post-cursor rays	N_b	8

Tab. 2. Summary of the intra cluster time domain parameters for the conference room channel model.

9. Conclusion

Design and standardization of 60 GHz WLAN systems require development of statistical channel models being able to reliably predict the propagation of the millimeter-wave signals in the interesting deployment scenarios. In this work, a statistical channel model for the indoor 60 GHz WLAN propagation channel in the office conference room environment is proposed. The channel model is designed to accurately predict the space-time channel characteristics with taking into account several properties especially important for 60 GHz WLANs deployment and operation. Those properties include explicit modeling of the azimuth and elevation angles of departure and arrival for every ray of the channel realization, support

of any type of the directional antenna technology like non-steerable antennas, sector-switched antennas, and adaptive antenna arrays, support of clustering of the 60 GHz indoor channel being a consequence of the quasi-optical propagation nature, and accurate prediction of the channel polarization characteristics.

To develop the channel model, a general mathematical structure required to represent all the needed model characteristics is introduced first. Then different aspects of the channel model are explained by presenting the corresponding channel modeling methodology for each aspect and continuing with development of the related parameters for the conference room channel model. The bases for the conference room channel model development are the experimental measurements performed in the conference room environment [1], [2], and ray-tracing simulations done for the conference room scenario.

The conference room channel model was recognized as meeting the 60 GHz WLAN development requirements and was accepted by the IEEE 802.11ad standardization committee for 60 GHz WLANs [4]. The proposed channel modeling methodology was reused for development of the channel models for two additional deployment scenarios – office cubicle environment and home living room [4], [6].

References

- [1] MALTSEV, A., MASLENNIKOV, R., SEVASTYANOV, A., KHORYAEV, A., LOMAYEV, A. Experimental investigations of 60 GHz wireless systems in office environment. *IEEE J. Selected Areas in Communications*, 2009, vol. 27, no. 8, p.1488-1499.
- [2] MALTSEV, A., PERAHIA, E., MASLENNIKOV, R., SEVASTYANOV, A., LOMAYEV, A., KHORYAEV, A. Impact of polarization characteristics on 60 GHz indoor radio communication systems. *IEEE Antennas and Wireless Propagation Letters*, 2010, vol. 9, p. 413 – 416.
- [3] XU, H., KUKSHYA, V., RAPPAPORT, T. S. Spatial and temporal characteristics of 60 GHz indoor channels. *IEEE Journal on Selected Areas in Communications*, 2002, vol. 20, no. 3, p. 620–630.
- [4] MALTSEV, A., et al. Channel models for 60 GHz WLAN systems. *IEEE Document* 802.11-09/0334r8, May 2010. Available at: <https://mentor.ieee.org/802.11/dcn/09/11-09-0334-08-00ad-channel-models-for-60-ghz-wlan-systems.doc>.
- [5] SALEH, A., VALENZUELA, R., A statistical model for indoor multipath propagation. *IEEE Journal on Selected Areas in Communications*, 1987, vol. 5, no. 2, p. 128-137.
- [6] PERAHIA, E., TGad Evaluation Methodology. *IEEE Document* 802.11-09/0296r16, January 2010. Available at: https://mentor.ieee.org/802.11/documents?is_dcn=296&is_group=00ad.
- [7] JACOB, M., et al. Modeling the dynamical human blockage for 60 GHz WLAN channel models. *IEEE Document* 802.11-10/0090r0, January 2010. Available at: https://mentor.ieee.org/802.11/documents?is_dcn=90&is_group=00ad.
- [8] JACOB, M. et al. A Ray tracing based stochastic human blockage model for the IEEE 802.11ad 60 GHz channel model. In *Proceedings of European Conference on Antennas and Propagation*, 2011, 5p.
- [9] JACKSON, J. D. *Classical Electrodynamics*. 3rd ed.), New York: Wiley, 1998.
- [10] MALTSEV, A., et al. Polarization model for 60 GHz. *IEEE Document*. 802.11-09/0431r0, April 2009. Available at: https://mentor.ieee.org/802.11/documents?is_dcn=431&is_group=00ad.
- [11] MALTSEV, A., et al. Verification of polarization impact model by experimental data. *IEEE Document* 802.11-09/1011r0, September 2009. Available at: https://mentor.ieee.org/802.11/documents?is_dcn=1011&is_group=00ad.
- [12] SATO, K., et al. Measurements of reflection and transmission characteristics of interior structures of office building in the 60 GHz band. *IEEE Trans. Antennas Propag.*, 1997, vol. 45, no. 12., p. 1783-1792.
- [13] DAVYDOV, A., et al., Saleh-Valenzuela channel model parameters for library environment. *IEEE Document* 802.15-06-0302-02-003c., July 2006. Available at: https://mentor.ieee.org/802.15/documents?is_dcn=302&is_group=003c.
- [14] SAWADA, H., et al. Intra-cluster response model and parameter for channel modelling at 60 GHz (Part 3). *IEEE Document* 802.11-10/0112r3, January 2010. Available at: https://mentor.ieee.org/802.11/documents?is_dcn=112&is_group=00ad.

About Authors

Alexander MALTSEV was born in Nizhny Novgorod, Russia in 1946. He received the Candidate of Science degree in 1975 and the Doctor of Science degree in 1990 all in radiophysics from the University of Nizhny Novgorod. From 1994 till present, he holds the position of Head of the Dept. of Bionics and Statistical Radiophysics of the University. In April 2001 Prof. Maltsev joined Intel Corporation. From April 2006 till present Alexander Maltsev is an Intel Principal Engineer managing Advanced Development team. Prof. Maltsev holds 30 US patents with about 40 patent filings. His research interests include optimal and adaptive statistical signal processing, adaptive antenna arrays, adaptive active vibration and noise control, space-time signal processing in non-stationary environment, MIMO-OFDM communication systems including Wi-Fi and WiMAX.

Roman MASLENNIKOV was born in Nizhny Novgorod, Russia in 1980. He received M.S. degree in radiophysics from the University of Nizhny Novgorod in 2002. From 2003 to 2009, Roman was with Intel Corporation, working on Wi-Fi and WiMAX communication systems development. Since 2009, he is technical manager for the Wireless Competence Center of the University of Nizhny Novgorod. His research interests include signal processing for wireless communication systems, multiple antenna algorithms, and communication systems simulations and prototyping.

Artyom LOMAYEV was born in 1983 in Nizhny Novgorod, Russia. He received his M.S. degree in radiophysics from the University of Nizhny Novgorod in 2005. His research interests include channel modeling, PHY algorithms design, Link Level Simulations (LLS) for wireless communication systems. Currently he holds the position of a Research Scientist at Intel Corporation.

Alexey SEVASTYANOV was born in Pavlovo, Russia in 1982. He received his M.S. degree in electrical engineering from the University of Nizhny Novgorod in 2005. Since 2006, he has been working as a research scientist in the Mobile Wireless Group, Intel Nizhny Novgorod Lab, Nizhny Novgorod, Russia. His research interests include communication systems prototyping, wireless propagation channel measurements and modeling, design of antenna systems for wireless communications.

Alexey KHORYAEV was born in Dzerzhinsk, Russia in 1980. He received his M.S. from the Radiophysics Faculty, University of Nizhny Novgorod, Russia in 2002. Since 2003, Alexey has been working as a senior research scientist in the wireless standards and technology group of Intel Nizhny Novgorod Lab. His research interests are in the areas of physical layer design for communication systems, digital signal processing algorithms, MIMO technologies, and hardware architectures.

RADIOENGINEERING REVIEWERS I

June 2011, Volume 20, Number 2

- AGGELIS, A., Democritus Univ. of Thrace, Greece
- ARCE-DIEGO, J. L., University of Cantabria, Santander, Spain
- ARTHABER, H., Vienna University of Technology, Austria
- BALLING, P., Antenna Systems Consulting ApS, Denmark
- BALTZIS, K., Aristotle University of Thessaloniki, Greece
- BAROŇÁK, I., Slovak University of Technology, Bratislava, Slovakia
- BÁRTÍK, H., Czech Technical University in Prague, Czechia
- BEŠŤÁK, R., Czech Technical University in Prague, Czechia
- BEZPALEC, P., Czech Technical Univ. in Prague, Czechia
- BIOLEK, D., University of Defense, Brno, Czechia
- BOBULA, M., RACOM company, Czechia
- BONEFAČIĆ, D., University of Zagreb, Croatia
- BRANČÍK, L., Brno Univ. of Technology, Czechia
- BURDA, K., Brno Univ. of Technology, Czechia
- CHAUDRY, A., Panjab University, India
- CHMELARŇ, M., Brno Univ. of Technology, Czechia
- COSTANZO, S., University of Calabria, Italy
- ČERNÝ, P., Czech Technical University in Prague, Czechia
- ČÍKA, P., Brno Univ. of Technology, Czechia
- DEL-RIO, C., University of Navarra, Spain
- DJIGAN, V., R&D Center of Microelectronics, Russia
- DOBEŠ, J., Czech Technical University in Prague, Czechia
- DORDOVÁ, J., Brno Univ. of Technology, Czechia
- DROTÁR, P., Honeywell International, Czechia
- DRUTAROVSKÝ, M., Technical University of Košice, Slovakia
- DŘÍNOVSKÝ, J., Brno Univ. of Technology, Czechia
- DVORSKÝ, M., VŠB - Technical University of Ostrava, Czechia
- DVOŘÁK, J., Brno Univ. of Technology, Czechia
- ELHADJ, Z., University of Tébessa, Algeria
- EOIN, T., University College Cork, Ireland
- FANJUL-VÉLEZ, F., University of Cantabria, Spain
- FLIEGEL, K., Czech Technical University in Prague, Czechia
- FRANEK, O., Aalborg University, Denmark
- GAI, Y., University of Southern California, USA
- GALAJDA, P., Technical Univ. of Košice, Slovakia
- GAZDA, J., Technical University of Košice, Slovakia
- GEORGIADIS, A., Centre Tecnologic de Telecomunicacions de Catalunya, Barcelona, Spain
- GOŇA, S., Tomas Bata University in Zlin, Czechia
- GRGIĆ, S., University of Zagreb, Croatia
- HAJNÝ, J., Brno Univ. of Technology, Czechia
- HANÁČEK, P., Brno Univ. of Technology, Czechia
- HAZDRA, P., Czech Technical University in Prague, Czechia
- HÁJEK, K., University of Defense, Brno, Czechia
- HÁZE, J., Brno Univ. of Technology, Czechia
- HEKRDLA, M., Czech Technical University in Prague, Czechia
- HENNIGER, H., German Aerospace Center, Germany